

Probabilistic Symmetry for Multi-Agent Dynamics

Sophia Sun

University of California, San Diego

SOPHIASUN@ENG.UCSD.COM

Robin Walters

Northeastern University

R.WALTERS@NORTHEASTERN.EDU

Jinxi Li

Hong Kong Polytechnic University

JINXI.LI@CONNECT.POLYU.HK

Rose Yu

University of California, San Diego

ROSEYU@UCSD.EDU

Editors: N. Matni, M. Morari, G. J. Pappas

Abstract

Learning multi-agent dynamics is a core AI problem with broad applications in robotics and autonomous driving. While most existing works focus on deterministic prediction, producing probabilistic forecasts to quantify uncertainty is critical for downstream decision-making tasks such as motion planning and collision avoidance. By leveraging the internal symmetry in multi-agent dynamics, specifically rotational equivariance, we can improve not only the accuracy, but also calibration of our probabilistic forecasts. We propose a novel deep dynamics model, Probabilistic Equivariant Continuous CONvolution (PECCO) for probabilistic prediction of multi-agent trajectories. PECCO extends equivariant continuous convolution to model the joint velocity distribution of multiple agents. It uses dynamics integration to propagate the uncertainty from velocity to position. We introduce Energy Score, a proper scoring rule, to evaluate probabilistic predictions. On both synthetic and real-world datasets, PECCO shows significant improvements in accuracy and calibration compared to non-equivariant baselines.

Our code is released at <https://github.com/Rose-STL-Lab/PECCO>. The appendix of the paper can be accessed at <https://arxiv.org/abs/2205.01927>.

Keywords: Multi-Agent Modeling, Probabilistic forecasting, deep dynamics model, uncertainty quantification, equivariant neural networks

1. Introduction

Predicting the future trajectory of multiple agents is a critical task with applications in autonomous driving (Chang et al., 2019), social behavioral modeling (Sun et al., 2021). In practice, the problem is difficult due to the inherent stochasticity of human motion, and the strong inter-dependency among the agents where the number of interactions grows quadratically with the number of agents. Moreover, agent movements are often influenced by environmental features such as road markings, boundaries, and social preference, which are impossible to measure and model effectively. Such a partially observed setting introduces a significant amount of uncertainty.

Many recent works on learning multi-agent dynamics has shifted to probabilistic modeling as a principled framework to represent uncertainty (Tang and Salakhutdinov, 2019; Salzman et al., 2020). However, common metrics used in probabilistic trajectory predictions works, such as minimum

average displacement of 6 samples (minADE) , do not fully reflect the quality of probabilistic forecasts. A probabilistic prediction should be *calibrated* and *sharp*; that is, the predicted distribution must cover likely future scenarios without being so broad and uncertain as to be useless.

In this paper, we propose a **Probabilistic Equivariant Continuous CO**nvolutional model (PECCO). PECCO is an equivariant probabilistic trajectory prediction model. Our key insight is to exploit *symmetry* to estimate multidimensional conditional distributions with limited data. We assume the predicted probability distribution is rotation and translation equivariant. That is, if the input data is transformed, the probability distribution will also be likewise transformed.

In Figure 1, we see the same car approaching an intersection from either the south or east. The scenes are related by a $\pi/2$ rotation. As the absolute compass direction is not particularly meaningful for local trajectory prediction, the model should thus output the same probability distributions over future trajectories for the car coming from the east as that coming from the north, but rotated by $\pi/2$. Rotational equivariance not only allows our model to produce physically consistent predictions, the multiplicative nature of equivariance also allows us to model a probability space with a smaller sample size (Bloem-Reddy and Teh, 2020). For each sample which an equivariant model is trained on, an equivariant model learns as if it were trained on all transformations of that sample by the symmetry group (Wang et al., 2021).

PECCO also mitigates issues posed by other methods for enforcing equivariance such as data augmentation and normalization. Data augmentation adds rotated versions of data samples to the training dataset such that the model learns rotational equivariance. However, this slows training drastically, requires greater model capacity, and rarely achieves the level of equivariance or accuracy as equivariant neural networks (Salzmann et al., 2020). Data normalization is a technique that rotates the scene to the agent’s reference frame for each data sample, as in Gao et al. (2020). However, in the multi-agent setting, it is impossible to rotate the scene for multiple agents without a canonical reference frame. PECCO allows the weights to be relative to the local orientation of each agent without the need to rotate the scene repeatedly.

Our main contributions are two folds: (1) We design an equivariant neural network, PECCO, for probabilistic forecast of multi-agent dynamics, and (2) we demonstrate that by incorporating symmetry, PECCO improves both calibration and sharpness of probabilistic forecasts on a synthetic particle dataset and two real-world benchmark datasets.

2. Related Work

Trajectory Prediction. Multi-agent trajectory forecasting has been extensively studied, approaches ranged from Kalman filters (Kalman, 1960) to non-linear Gaussian Process Regression models (Jordan, 1998). However, these methods either rely on strong assumptions of the dynamics, or do not explicitly model multi-agent interactions. We refer readers to Rudenko et al. (2020) for

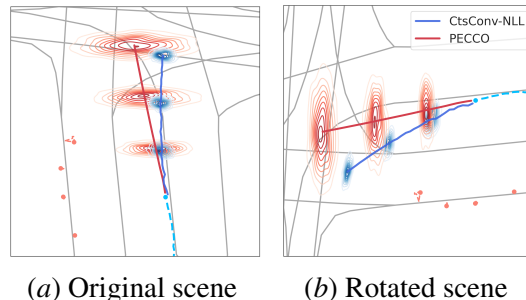


Figure 1: Prediction on the same scene rotated by 90 degrees. PECCO is consistent in trajectory and uncertainty prediction, whereas the non-equivariant model (CtsConv) fails.

a comprehensive survey of such methods. Advancements in deep learning have allowed flexible modeling of trajectory dynamics (Alahi et al., 2016; Wang et al., 2018; Deo and Trivedi, 2018; Sadeghian et al., 2019; Liang et al., 2020; Walters et al., 2021; Gao et al., 2020; Roddenberry et al., 2021), but they focus mainly on point estimation without uncertainty.

Recent methods have shifted to predicting distributions of future trajectories, capturing uncertainty in dynamics. There are two main categories for probabilistic forecasting: (1) *explicitly* via exact likelihood (Tang and Salakhutdinov, 2019; Chai et al., 2019; Gu et al., 2021) and variational inference (Sohn et al., 2015; Salzman et al., 2020; Lee et al., 2017), or (2) *implicitly* with Generative Adversarial Networks (GANs) (Gupta et al., 2018; Liu et al., 2019). Our work falls into the first category where we model the distributions parametrically. Parametric models allow us to evaluate the likelihood of future trajectories, which are useful for downstream planning tasks (Chai et al., 2019; Schwarting et al., 2018).

Despite the development in probabilistic modeling, there is no standard metric for quantifying uncertainty of the prediction. Negative log likelihood often overfits the distribution (Guo et al., 2017), and best-of-n-sample results do not evaluate the full distribution (Ivanovic and Pavone, 2021). We argue that probabilistic forecasts should accurately reflect the uncertainty in the model predictions. We propose using proper scoring rules such as Energy Score or mean interval score (Gneiting and Raftery, 2007) for evaluating probabilistic forecasts.

Equivariant Deep Learning. Geometric deep learning that leverages invariance and symmetries has found wide applications in areas ranging from image recognition (Bao and Song, 2019; Worrall et al., 2017; Weiler and Cesa, 2019) to reinforcement learning (van der Pol et al., 2020). Equivariant neural networks are studied for modeling dynamics as well - Fuchs et al. (2020) use SE(3)-equivariant transformers to predict trajectories for a small number of particles as a regression task, and Walters et al. (2021) proposed a S0(2) equivariant continuous convolution for traffic trajectory prediction. All the methods mentioned above are deterministic. Köhler et al. (2020) and Satorras et al. (2021) studies equivariant normalizing flows for modeling symmetric densities, however their domains focus on generative modeling and therefore differ from our work significantly. To our knowledge, no previous work has studied equivariant neural networks for probabilistic dynamics forecasting.

Uncertainty Quantification (UQ). Uncertainty quantification is critical for risk assessment in safety-critical domains. Properly quantified uncertainties can be used to create probabilistic constraints and generate more robust planning and control strategies (Ostafew et al., 2016; Bujarbaruah et al., 2019). With the increasing use of deep learning in forecasting tasks, many works have UQ for neural networks (Luo et al., 2021; Wu et al., 2021; Guo et al., 2017). Stankevičiūtė et al. (2021) proposes a conformal prediction algorithm for 1D RNN forecasters with a prediction region with coverage guarantees. However, these works focus only on classification or 1-dimensional forecasts. Salinas et al. (2019, 2020) use autoregressive RNNs for probabilistic forecasting of multiple time series, however, their method cannot explicitly model spatial relations. We present a model design for multi-agent dynamics and produce probabilistic distributions with better calibration.

3. Background

We give a short background on symmetry and equivariance and their probabilistic extension.

Symmetry and Equivariance. A *symmetry group* G is a set together with a composition operation $\circ: G \times G \rightarrow G$ which is associative and has an identity and inverses. The group G can transform a

vector space V by specifying a *representation* which is a mapping $\rho: G \rightarrow \text{GL}_n(V)$ sending each element of the group G to an invertible $n \times n$ matrix such that $\rho(g_1 \circ g_2) = \rho(g_1)\rho(g_2)$.

Given a function $f: X \rightarrow Y$ such that G has representations ρ_X and ρ_Y acting on X and Y respectively, we say f is *G-equivariant* if for all $x \in X$ and $g \in G$, we have $\rho_Y(g)f(x) = f(\rho_X(g)x)$. That is, a transformation of the input of x induces a corresponding transformation of the output. *Invariance* for the function f is a special case in which $\rho_Y(g)y = y$.

SO(2) Equivariant Continuous Convolution. Continuous convolution (Ummenhofer et al., 2019) generalizes discrete convolution. The feature vector $\mathbf{f}^{(i)} \in \mathbb{R}^{c_{\text{in}}}$ of particle i forms a vector field \mathbf{f} , and the kernel of the convolution $K: \mathbb{R}^2 \mapsto \mathbb{R}^{c_{\text{out}} \times c_{\text{in}}}$ forms a matrix field: for each point $\mathbf{x} \in \mathbb{R}^2$, $K(\mathbf{x})$ is a $c_{\text{out}} \times c_{\text{in}}$ matrix. The continuous convolution is then defined by

$$\mathbf{g}^{(i)} = \sum_j a(\|\mathbf{x}^{(j)} - \mathbf{x}^{(i)}\|)K(\mathbf{x}^{(j)} - \mathbf{x}^{(i)}) \cdot \mathbf{f}^{(j)}.$$

By Weiler and Cesa (2019), this is SO(2)-equivariant if $K(gv) = \rho_{\text{out}}(g)K(v)\rho_{\text{in}}(g^{-1})$.

ECCO (Walters et al., 2021) defines the convolution kernel K in polar coordinates $K(\theta, r)$. Let $\mathbb{R}^{c_{\text{in}}}$ and $\mathbb{R}^{c_{\text{out}}}$ be SO(2)-representations ρ_{in} and ρ_{out} respectively, then the convolution kernel satisfies the equivariance condition as follows, making the continuous convolution SO(2)-equivariant.

$$K(\theta + \phi, r) = \rho_{\text{out}}(\text{Rot}_\theta)K(\phi, r)\rho_{\text{in}}(\text{Rot}_\theta^{-1})$$

Calibration and Sharpness of Probabilistic Prediction. It is desirable for a probabilistic prediction to be both *calibrated* and *sharp*. A model is *calibrated* when the predicted probability correspond to the true probability of an event. In forecasting, calibration is often measured with *coverage*, the probability of ground truth Y falls into prediction region of confidence $\hat{C}^{1-\alpha}$, $1 - \alpha \in [0, 1]$.

$$P(Y \in \hat{C}^{1-\alpha}) \geq 1 - \alpha \quad (1)$$

Note that one can always obtain a calibrated prediction region by setting $\hat{C}^{1-\alpha}$ to be the entire Y space. We introduce the concept of *Sharpness*, which refers to the size of the prediction region $|\hat{C}^{1-\alpha}|$. The balance between calibration and sharpness can be measured by a class of metrics called proper scoring rules (Gneiting and Raftery, 2007).

4. PECCO

4.1. Problem Setup

Given past trajectories of n agents over t time steps $\{x_j^{(1)}, x_j^{(2)}, \dots, x_j^{(n)}\}_{j=1}^t$, where $x_j^{(i)} \in \mathbb{R}^2$, and the environmental context information \mathbf{e} including marker positions of map lane boundaries, we model the probability distribution of agents' positions over k future time steps as $p_\theta(x_{t+1:t+k} | x_{1:t}, \mathbf{e})$, with $x_j = (x_j^{(1)}, \dots, x_j^{(n)})$ being the positions of all agents at time step j . We introduce PECCO, a deep learning model that leverages rotational equivariance to produce probabilistic forecasts.

The high-level architecture of our model is illustrated in Figure 2. PECCO takes as input the positions of all agents $x_{1:t}$ in the past, and the covariance matrix $\Sigma_{x,j}$ at time j . It outputs the probability distribution of each agents' velocity as a 2-D Gaussian $\mathcal{N}(\mu_{v,j+1}^{(i)}, \Sigma_{v,j+1}^{(i)})$ for the next time step. The velocity distribution is then integrated into a position distribution $\mathcal{N}(\mu_{x,j+1}^{(i)}, \Sigma_{x,j+1}^{(i)})$ through dynamics integration. PECCO predicts the future k timesteps autoregressively. The output distributions are guaranteed to be rotational equivariant by our model implementation.

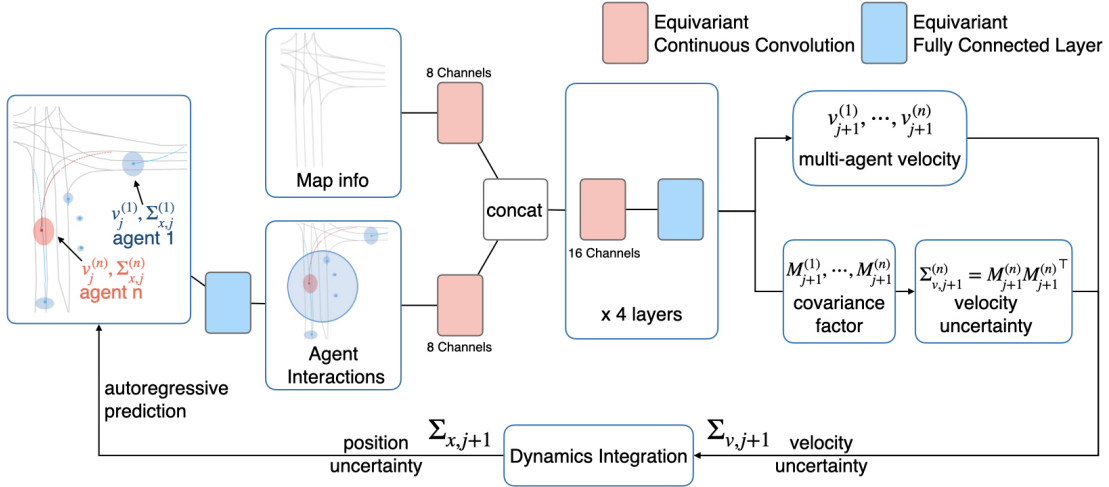


Figure 2: Overview of PECCO’s model architecture. Agent trajectories consisting of velocities and position uncertainties are encoded along with map information by equivariant continuous convolution and fully connected layers. The model outputs v_{j+1} and $\Sigma_{v,j+1}$ for all agents, which we use to calculate position uncertainty $\Sigma_{x,j+1}$ via dynamics. The model takes in the forecast and predicts autoregressively.

4.2. Probabilistic Symmetry through Equivariant Neural Networks

Rotational equivariance effectively reduces the dimension of the data space by placing different samples in the same equivalence class. This improves data coverage for better probabilistic modeling.

Intuitively, real-world trajectory dynamics has intrinsic symmetry. That is, if past trajectories and environmental data such as the map is rotated, then the probability of a rotated future trajectory will be equally likely. We can model the probability density function p_θ as an invariant function of its inputs as in Equation 2. Here, each past and future position $x_j^{(i)} \in \mathbb{R}^2$ is transformed according the standard representation ρ_1 .

$$p_\theta(x_{t+1:t+k}|x_{1:t}, \mathbf{e}) = p_\theta(gx_{t+1:t+k}|gx_{1:t}, g\mathbf{e}) \quad \forall g \in \text{SO}(2) \quad (2)$$

In order to implement Equation 2, we assume future positions follow a multivariate normal distribution $x_j^{(i)} \sim N(\mu_{x,j}^{(i)}, \Sigma_{x,j}^{(i)})$. This is a common assumption in trajectory forecasting literature (Rudenko et al., 2020) and provides a convenient parametric form for optimization and reasoning. In the following expositions we omit the underscore x for simplicity.

We aim to construct an equivariant neural network f_θ that outputs the parameters $\mu_j^{(i)}$ and $\Sigma_j^{(i)}$ autoregressively, taking as input probability distributions over the positions of all agents in the past k time steps

$$\mu_{j+1}, \Sigma_{j+1} = f_\theta(\mu_{j-t+1:j}, \Sigma_{j-t+1:j}, \mathbf{e}).$$

where $\mu_j = (\mu_j^{(1)}, \dots, \mu_j^{(n)})$ and $\Sigma_j = (\Sigma_j^{(1)}, \dots, \Sigma_j^{(n)})$ and \mathbf{e} denotes environmental information.

In this case, the equivariance of f_θ leads to the desired invariance of p_θ . This may be seen as a partial evaluation or currying of the conditional probability density function which has the effect of transforming invariance to equivariance. The following proposition relates equivariant networks with probabilistic symmetry. See Appendix A for a proof.

Proposition 1 (One step equivariance implies n -step equivariance) *If the one-step probabilistic forecasting model f_θ is G -equivariant, then the probability distribution $p_\theta(x_{t+1:t+k}|x_{1:t}, \mathbf{e})$ is invariant as in Equation 2.*

In order to enforce $\text{SO}(2)$ -equivariance for f_θ , the following proposition describes how the mean and covariance matrix for a 2-D Gaussian transforms under a rotation of \mathbb{R}^2 .

Proposition 2 (SO(2) equivariance of multivariate Gaussian) *Given multivariate normal distribution $\mathcal{N}(\mu, \Sigma)$ over \mathbb{R}^2 with probability density function $p_{\mu, \Sigma}$ and $g \in \text{SO}(2)$, then $\mathcal{N}(g\mu, g\Sigma g^T)$ is also a multivariate normal distribution and $p_{g\mu, g\Sigma g^T}(v) = p_{\mu, \Sigma}(g^{-1}v)$ for all $v \in \mathbb{R}^2$.*

To ensure the covariance matrix of f_θ is positive-definite and symmetric, i.e. $\Sigma \in \text{PosDefSym}_2(\mathbb{R})$, we make use of the following fact:

Proposition 3 (Equivariant maps constructing positive-definite symmetric matrices) *The map*

$$\varphi: \text{GL}_2(\mathbb{R}) \rightarrow \text{PosDefSym}_2(\mathbb{R}), \quad M \mapsto MM^T \quad (3)$$

is surjective and equivariant. That is, for $g \in \text{SO}(2)$ we have

$$\varphi(gM) = g\varphi(M)g^T. \quad (4)$$

Moreover, φ admits a one-sided inverse which is also equivariant,

$$\psi: \text{PosDefSym}_2(\mathbb{R}) \rightarrow \text{GL}_2(\mathbb{R}), \quad \Sigma \mapsto Q\Lambda^{\frac{1}{2}} \quad (5)$$

where $Q\Lambda Q^T$ is the eigendecomposition of Σ and Q is orthogonal. Together, $\varphi(\psi(\Sigma)) = \Sigma$.

As a consequence of Proposition 2 and Proposition 3, we can ensure that the predicted distribution transforms correctly under equivariance by (1) predicting an intermediate matrix M for covariance, and (2) constraining \tilde{f}_θ to be equivariant with respect to the action in Equation 4.

$$\mu_{j+1}, M_{j+1} = \tilde{f}_\theta(\mu_{j-k:j}, M_{j-k:j}, \mathbf{e}), \quad \Sigma_{j+1} = M_{j+1}M_{j+1}^T \quad (6)$$

In this case, $\text{SO}(2)$ acts by transforming the the columns of M independently as vectors in \mathbb{R}^2 . Thus the data $(\mu_j^{(i)}, \Sigma_j^{(i)})$ for each agent and time step is comprised of 3 copies of the standard representation ρ_1 as defined in Section 3. Given this $\text{SO}(2)$ action, we can enforce $\text{SO}(2)$ -equivariance in the neural network \tilde{f}_θ . Implementation details of of the equivariant layers are provided in Appendix B.

4.3. Dynamics Integration (dyna)

Instead of predicting the position directly, PECCO outputs a Gaussian distribution over *velocity* as $\mathcal{N}(\mu_{v,j}, \Sigma_{v,j})$. More specifically, it predicts $(\mu_{v,j}, M_{v,j})$ at each time step and the covariance matrix $\Sigma_{v,j}$ is calculated as in Proposition 3. However, we want to obtain the uncertainty over *position* as $\Sigma_{x,j}$ and perform autoregressive forecasting. We leverage dynamics integration to propagate the uncertainty from velocity to position.

Assuming that all agents in the system can be approximated as linear discrete time dynamics $x_{j+1} = x_j + \Delta t \cdot v_j$, we can obtain the uncertainty of predicted position $\Sigma_{x,j+1}$ by

$$\Sigma_{x,j+1} = \Sigma_{x,j} + (\Delta t)^2 \Sigma_{v,j} + 2\Delta t \cdot \text{cov}(x_j, v_j).$$

We assume that the cross covariance matrix $\text{cov}(x_j, v_j)$ is zero for simplicity following previous works (Salzmann et al., 2020). During training, gradients are calculated after entire trajectory is predicted autoregressively. A consequence of the additive uncertainty setup is that it enforces the uncertainty to grow monotonically over time, creating a ‘‘cone of uncertainty’’.

5. Experiments

We show that our model produces accurate and more calibrated probabilistic forecast compared to baseline models on one synthetic and two real world trajectory prediction datasets: interacting particles, autonomous vehicle, and pedestrian movement.

5.1. Baselines

- LSTM-NLL (variation of Alahi et al. (2016)): An encoder-decoder LSTM model that predicts the mean and variance of a Gaussian distribution, optimizing likelihood of data. We also train a version with random rotation data augmentation LSTM-aug.
- CtsConv (Ummenhofer et al., 2019): Continuous convolution over point cloud data for trajectory prediction, a non-equivariant counterpart of PECCO. CtsConv-aug is trained with a data augmentation step where we randomly rotate the scenes.
- Multiple Futures Prediction (MFP) (Tang and Salakhutdinov, 2019): A encoder-decoder model for multimodal probabilistic trajectory forecasts.
- Trajectron++ (Salzmann et al., 2020): State-of-the-art probabilistic trajectory prediction model with graph representation of agent interactions and conditional VAE architecture.

5.2. Evaluation Metrics.

- *Minimum Average/Final Displacement Error* (minADE₆, minFDE₆): average l_2 displacement error over k steps, or average displacement of the final step, between predicted and ground truth trajectories. We report the minimum over 6 samples for probabilistic models.
- *Negative Log Likelihood* (NLL): NLL of ground truth trajectories under predicted distributions.
- *Energy Score* (ES) (Gneiting and Raftery, 2007): a proper scoring rule to measure calibration and sharpness of the predicted distribution P . The energy score for a distribution P and the ground truth data x is defined as: $\text{ES}(P, x) = E_{X \sim P} \|X - x\| - \frac{1}{2} E_{X, X' \sim P} \|X - X'\|$. Here X and X' are independent samples from P .
- *Coverage*: The empirical estimate of probability of the true value lying in the predicted interval, defined in equation 1. We report the coverage of 90% quantile of the predicted Gaussian. The prediction is more *calibrated* if the coverage is closer to 90%.

5.3. Datasets.

The particle dataset is a synthetic dataset of 5 particles interacting in spring dynamics (Kipf et al., 2018) with dynamics noise. The models predict 20 time steps given 30 steps as input. The Argoverse autonomous vehicle motion forecasting (Chang et al., 2019) is a widely used vehicle trajectory prediction benchmark. The task is to predict 3 second trajectories based on all vehicle history in the past 2 seconds recorded at 10Hz. TrajNet++ (Sadeghian et al., 2018) is a popular pedestrian

Model	minADE ₆ ↓	minFDE ₆ ↓	NLL ↓	ES ↓	Cov@1s(%)	Cov@2s	Cov@3s
Argoverse							
LSTM-NLL	1.64 ± .05	4.17 ± .10	3.07 ± .08	2.31 ± .54	8.8 ± 0.7	8.5 ± 0.7	7.0 ± 0.8
LSTM-NLL-aug	1.61 ± .02	4.15 ± .08	2.78 ± .03	1.99 ± .46	10.1 ± 1.5	10.5 ± 1.0	9.8 ± 1.9
CtsConv-NLL	1.74 ± .03	4.43 ± .06	29.1 ± 2.2	6.71 ± .70	6.3 ± 2.2	0.02 ± .01	0.01 ± .01
CtsConv-NLL-aug	1.66 ± .02	4.23 ± .06	11.81 ± .01	5.10 ± .35	11.9 ± 2.1	1.7 ± 0.5	0.02 ± .01
Trajectron++	1.83 ± .02	3.85 ± .07	2.48 ± .27	3.92 ± .61	45.5 ± 5.3	37.6 ± 3.2	34.9 ± 2.5
MFP	1.53 ± .04	3.77 ± .06	3.56 ± .02	2.33 ± .21	51.3 ± 5.1	33.0 ± 4.9	8.3 ± 4.8
PECCO	1.39 ± .02	3.41 ± .03	4.26 ± 0.1	1.54 ± .16	74.9 ± 0.6	78.6 ± 2.8	84.5 ± 2.9
TrajNet++							
LSTM-NLL-aug	0.85 ± .02	1.64 ± .03	2.78 ± .02	-0.28 ± .09	29.0 ± 4.3	23.2 ± 4.2	23.7 ± 3.9
CtsCov-NLL	1.08 ± .02	2.36 ± .09	5.33 ± .08	1.67 ± .13	43.8 ± 10.6	20.7 ± 5.2	12.2 ± 6.7
CtsCov-NLL-aug	0.92 ± .01	1.76 ± .03	6.74 ± .21	1.42 ± .11	62.1 ± 3.3	36.3 ± 4.9	34.1 ± 5.8
Trajectron++	1.14 ± .03	2.31 ± .05	2.83 ± .12	0.98 ± .17	50.2 ± 2.2	45.8 ± 3.5	32.9 ± 3.5
MFP	0.85 ± .02	1.70 ± .04	2.20 ± .04	0.67 ± .08	79.1 ± 4.3	32.5 ± 3.1	22.8 ± 3.2
PECCO	0.59 ± .12	1.06 ± .17	2.37 ± .04	-0.73 ± .10	80.8 ± 4.5	85.9 ± 2.3	94.5 ± 3.0

Table 2: Performance comparison on benchmark datasets Argoverse and TrajNet++. Cov@*ks*(%) refers to coverage at the *k* second mark; prediction is more *calibrated* if closer to 90%. PECCO is more accurate and calibrated compared to non-equivariant baseline models.

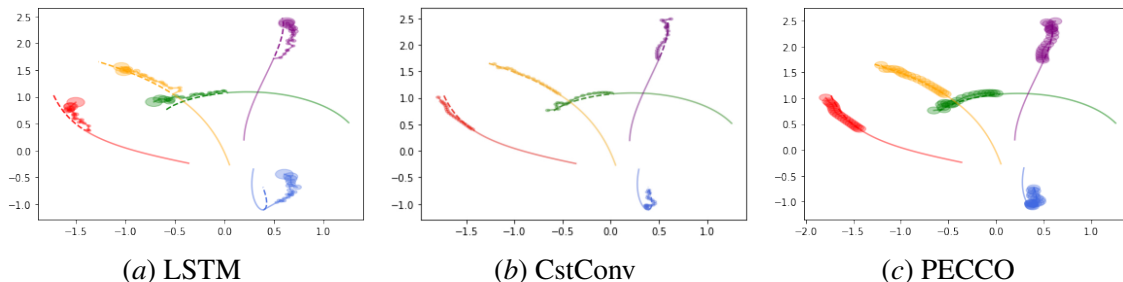


Figure 3: Comparison of prediction results between baselines. The solid lines are input timesteps to the models, the dotted lines ground truth, and the circles the 90% confidence regions. We can see that PECCO achieves accurate results while maintaining good coverage.

trajectory benchmark with a focus on agent-agent interaction scenarios. The task is to predict 12 time steps for agents given 9. We refer the reader to Appendix D.1 for data and training details.

5.4. Experimental Results

Particles dataset. We present experimental result for the synthetic particle dataset in Table 1. We visualize a test sample in Figure 3 to qualitatively illustrate PECCO’s improved accuracy and calibration.

Argoverse and TrajNet++. Table 2 presents experimental results on two benchmark datasets. PECCO achieves better regression accuracy compared to non-equivariant baseline in terms of minADE and minFDE, with a notable 9% improve-

Model	MSE ↓	NLL ↓	ES ↓
LSTM	.016	-1.61	1.041
CtsConv	.010	-0.81	0.667
PECCO	.004	-0.83	0.467

Table 1: PECCO outperforms baseline models in all metrics on the synthetic particles dataset.

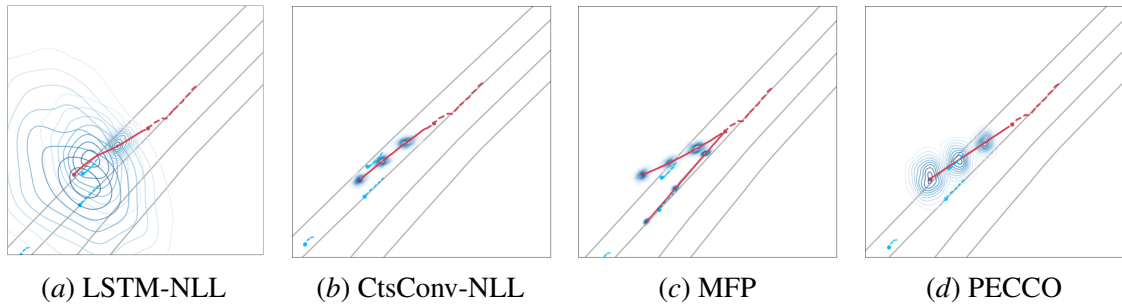


Figure 4: Comparison of uncertainty predicted at a lane change. Red trajectories are the agent of interest in the same scenario. Note how the LSTM predicted uncertainty explodes after a few time steps, while CtsConv and MFP has overconfident distributions. PECCO is able to model possibility of both staying and lane change.

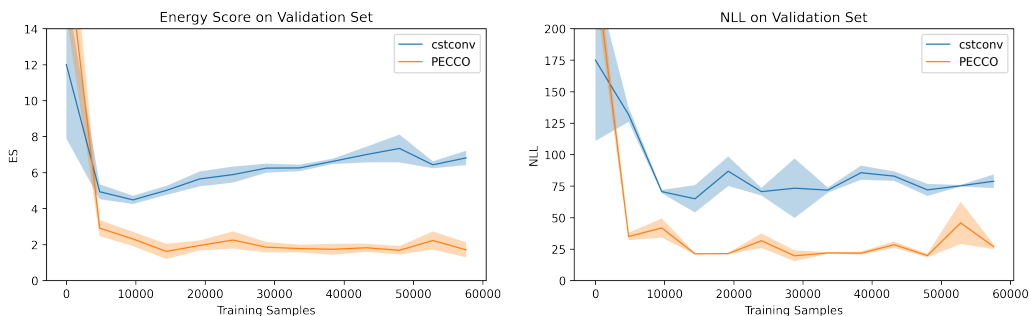


Figure 5: With equivariance, PECCO is able to achieve better energy score and NLL with fewer data samples, compared to its non-equivariant counterpart.

ment in minADE over the the best performing baseline, MFP.

PECCO’s improved probability coverage allows for more diverse sampling and hence can produce trajectories closer to ground truth.

PECCO’s probabilistic predictions are able to achieve consistently better coverage compared to other methods whose coverage deteriorates over time. Comparing LSTM-NLL and CtsConv-NLL with their augmented counterparts, LSTM-NLL-aug and CtsConv-NLL-aug, we can see that data augmentation through rotation improves both accuracy and calibration. PECCO leverages this symmetry to improve accuracy, maintain good calibration, and converge faster (Figure 5).

Figure 4 visualizes a typical situation to illustrate this difference. We plot the predicted distribution at 10, 20, and 30 time steps of prediction (1 time step is 0.1 seconds). We can see the probable region predicted by LSTM-NLL explodes at timesteps 20 and 30, whereas CtsConv-NLL and MFP tend to be overconfident in their predictions. PECCO is able to predict a Gaussian that covers both cases of staying in the lane and changing to the right lane.

5.5. Model Analysis

Comparison with data augmentation and canonicalization. Data augmentation and canonicalization are popular methods to implicitly exploit symmetry in trajectory data. In Table 4 we

Model	minADE ₆ ↓	minFDE ₆ ↓	MRS ↓	Cov@1s(%)	Cov@2s	Cov@3s
Conformal LSTM	2.45 ± 0.09	4.68 ± 0.15	198.1 ± 12.0	90.1 ± 0.1	92.7 ± 0.1	92.8 ± 0.1
Conformal ECCO	1.96 ± 0.06	4.32 ± 0.10	220.9 ± 8.1	90.0 ± 0.1	90.1 ± 0.1	90.0 ± 0.1
PECCO	1.39 ± .02	3.41 ± 0.03	8.52 ± 0.16	74.9 ± 0.2	93.6 ± 0.8	92.5 ± 0.9

Table 3: Comparison with conformal prediction methods on Argoverse dataset. PECCO produces a parametric distribution with a tighter confidence region (small MRS), whereby achieving better regression accuracy while maintaining competitive coverage.

compare PECCO to its nonequivariant counterparts with the addition of data augmentation and canonicalization. Equivariance dramatically improves prediction performance in all aspects, especially calibration.

Dynamics Integration Ablation. Dynamic integration (dyna) introduced in Section 4.3 enforces the uncertainty to grow monotonically over time. As an ablative study, Table 5 show that PECCO with dynamic integration has much better calibration compared to if without; for the Argoverse dataset, the improved calibration also informs better performance on minADE/FDE.

Comparison with Conformal Prediction. We compare to two conformal prediction baselines

(Stankevičiūtė et al., 2021) (Appendix C.3 for details) in Table 3. Conformal methods achieve guaranteed $\geq 90\%$ coverage, but suffer in prediction accuracy due to having to split training data for calibration. Since conformal prediction does not output a distribution, we use another proper scoring rule Mean Regional Score (2d extension of mean interval score in Gneiting and Raftery (2007), see Appendix B) as metric. The conformal regions are much larger (higher MRS), which is less desirable for downstream decision making tasks.

6. Conclusion

In this work we propose Probabilistic Equivariant Continuous Convolution (PECCO), a novel multi-agent probabilistic prediction method for improving uncertainty quantification. We design an equivariant neural network under which the predicted distributions transform correspondingly as inputs are transformed. We introduce the Energy Score metric to bring attention to the calibration of multivariate probabilistic forecasts. By leveraging equivariance, PECCO produces more accurate and calibrated probabilistic forecasts compared to existing methods on both synthetic and real-world datasets.

	minA/FDE ₆	NLL	Cov(%)
CtsConv	1.74 / 4.43	29.13	2.2
+cannon	1.66 / 4.28	17.46	4.5
+aug	1.67 / 4.23	11.81	17.1
equivariant	1.39 / 3.41	4.26	87.5

Table 4: Data Augmentation Comparison on the Argoverse Dataset.

Argoverse	minA/FDE ₆	NLL	Cov(%)
no-dyna	1.52 / 3.76	9.72	38.6
dyna	1.39 / 3.41	4.26	87.5
Pedestrian	minA/FDE ₆	NLL	Cov(%)
no-dyna	0.72 / 2.12	4.71	39.6
dyna	0.73 / 1.98	2.37	83.7

Table 5: Dynamics Integration (dyna) Ablation: using dyna encourages the uncertainty to grow over time and improves coverage.

Acknowledgments

This work was supported in part by U.S. Department Of Energy, Office of Science, Facebook Data Science Research Awards, U. S. Army Research Office under Grant W911NF-20-1-0334, and NSF Grants #2134274 and #2146343.

References

- Alexandre Alahi, Kratarth Goel, Vignesh Ramanathan, Alexandre Robicquet, Li Fei-Fei, and Silvio Savarese. Social lstm: Human trajectory prediction in crowded spaces. In *Proceedings of the IEEE conference on computer vision and pattern recognition*, 2016.
- Erkao Bao and Linqi Song. Equivariant neural networks and equivarification. *arXiv preprint arXiv:1906.07172*, 2019.
- Benjamin Bloem-Reddy and Yee Whye Teh. Probabilistic symmetries and invariant neural networks. *Journal of Machine Learning Research*, 21(90), 2020.
- Monimoy Bujarbaruah, Xiaojing Zhang, Marko Tanaskovic, and Francesco Borrelli. Adaptive mpc under time varying uncertainty: Robust and stochastic. *arXiv preprint arXiv:1909.13473*, 2019.
- Yuning Chai, Benjamin Sapp, Mayank Bansal, and Dragomir Anguelov. Multipath: Multiple probabilistic anchor trajectory hypotheses for behavior prediction. *arXiv preprint arXiv:1910.05449*, 2019.
- Ming-Fang Chang, John W Lambert, Patsorn Sangkloy, Jagjeet Singh, Slawomir Bak, Andrew Hartnett, De Wang, Peter Carr, Simon Lucey, Deva Ramanan, and James Hays. Argoverse: 3d tracking and forecasting with rich maps. In *Conference on Computer Vision and Pattern Recognition (CVPR)*, 2019.
- Nachiket Deo and Mohan M Trivedi. Convolutional social pooling for vehicle trajectory prediction. In *Proceedings of the IEEE Conference on Computer Vision and Pattern Recognition Workshops*, 2018.
- Fabian B Fuchs, Daniel E Worrall, Volker Fischer, and Max Welling. SE(3)-transformers: 3D roto-translation equivariant attention networks. *arXiv preprint arXiv:2006.10503*, 2020.
- Jiyang Gao, Chen Sun, Hang Zhao, Yi Shen, Dragomir Anguelov, Congcong Li, and Cordelia Schmid. Vectornet: Encoding hd maps and agent dynamics from vectorized representation. In *Proceedings of the IEEE/CVF Conference on Computer Vision and Pattern Recognition*, 2020.
- Tilmann Gneiting and Adrian E Raftery. Strictly proper scoring rules, prediction, and estimation. *Journal of the American statistical Association*, 102(477), 2007.
- Junru Gu, Chen Sun, and Hang Zhao. Densent: End-to-end trajectory prediction from dense goal sets. In *Proceedings of the IEEE/CVF International Conference on Computer Vision*, 2021.
- Chuan Guo, Geoff Pleiss, Yu Sun, and Kilian Q Weinberger. On calibration of modern neural networks. In *International Conference on Machine Learning*. PMLR, 2017.

- Agrim Gupta, Justin Johnson, Li Fei-Fei, Silvio Savarese, and Alexandre Alahi. Social gan: Socially acceptable trajectories with generative adversarial networks. In *Proceedings of the IEEE Conference on Computer Vision and Pattern Recognition*, 2018.
- Boris Ivanovic and Marco Pavone. Rethinking trajectory forecasting evaluation. *arXiv preprint arXiv:2107.10297*, 2021.
- Michael I. Jordan, editor. *Prediction with Gaussian Processes: From Linear Regression to Linear Prediction and Beyond*. The MIT Press, 1998.
- Rudolph Emil Kalman. A new approach to linear filtering and prediction problems. *Journal of Basic Engineering*, 82(1), 1960.
- Thomas Kipf, Ethan Fetaya, Kuan-Chieh Wang, Max Welling, and Richard Zemel. Neural relational inference for interacting systems. In *International Conference on Machine Learning*, pages 2688–2697. PMLR, 2018.
- Jonas Köhler, Leon Klein, and Frank Noé. Equivariant flows: exact likelihood generative learning for symmetric densities. In *International Conference on Machine Learning*. PMLR, 2020.
- Namhoon Lee, Wongun Choi, Paul Vernaza, Christopher B Choy, Philip HS Torr, and Manmohan Chandraker. Desire: Distant future prediction in dynamic scenes with interacting agents. In *Proceedings of the IEEE Conference on Computer Vision and Pattern Recognition*, 2017.
- Ming Liang, Bin Yang, Rui Hu, Yun Chen, Renjie Liao, Song Feng, and Raquel Urtasun. Learning lane graph representations for motion forecasting. In *European Conference on Computer Vision*. Springer, 2020.
- Yukai Liu, Rose Yu, Stephan Zheng, Eric Zhan, and Yisong Yue. Naomi: Non-autoregressive multiresolution sequence imputation. *Advances in Neural Information Processing Systems*, 2019.
- Rachel Luo, Shengjia Zhao, Jonathan Kuck, Boris Ivanovic, Silvio Savarese, Edward Schmerling, and Marco Pavone. Sample-efficient safety assurances using conformal prediction. *arXiv preprint arXiv:2109.14082*, 2021.
- Chris J Ostafew, Angela P Schoellig, Timothy D Barfoot, and Jack Collier. Learning-based nonlinear model predictive control to improve vision-based mobile robot path tracking. *Journal of Field Robotics*, 33(1), 2016.
- T Mitchell Roddenberry, Nicholas Glaze, and Santiago Segarra. Principled simplicial neural networks for trajectory prediction. In *International Conference on Machine Learning*. PMLR, 2021.
- Andrey Rudenko, Luigi Palmieri, Michael Herman, Kris M Kitani, Darius M Gavrilă, and Kai O Arras. Human motion trajectory prediction: a survey. *The International Journal of Robotics Research*, 39(8), 2020.
- Amir Sadeghian, Vineet Kosaraju, Agrim Gupta, Silvio Savarese, and Alexandre Alahi. Trajnet: Towards a benchmark for human trajectory prediction. *arXiv preprint*, 2018.

- Amir Sadeghian, Vineet Kosaraju, Ali Sadeghian, Noriaki Hirose, Hamid Rezaatofghi, and Silvio Savarese. Sophie: An attentive gan for predicting paths compliant to social and physical constraints. In *Proceedings of the IEEE/CVF Conference on Computer Vision and Pattern Recognition*, 2019.
- David Salinas, Michael Bohlke-Schneider, Laurent Callot, Roberto Medico, and Jan Gasthaus. High-dimensional multivariate forecasting with low-rank gaussian copula processes. *Advances in neural information processing systems*, 32, 2019.
- David Salinas, Valentin Flunkert, Jan Gasthaus, and Tim Januschowski. Deepar: Probabilistic forecasting with autoregressive recurrent networks. *International Journal of Forecasting*, 36(3): 1181–1191, 2020.
- Tim Salzmann, Boris Ivanovic, Punarjay Chakravarty, and Marco Pavone. Trajectron++: Dynamically-feasible trajectory forecasting with heterogeneous data. In *ECCV*. Springer, 2020.
- Victor Garcia Satorras, Emiel Hoogeboom, Fabian Bernd Fuchs, Ingmar Posner, and Max Welling. E (n) equivariant normalizing flows. In *Thirty-Fifth Conference on Neural Information Processing Systems*, 2021.
- Wilko Schwarting, Javier Alonso-Mora, and Daniela Rus. Planning and decision-making for autonomous vehicles. *Annual Review of Control, Robotics, and Autonomous Systems*, 1, 2018.
- Glenn Shafer and Vladimir Vovk. A tutorial on conformal prediction. *Journal of Machine Learning Research*, 9(3), 2008.
- MInoru Slotani. Tolerance regions for a multivariate normal population. *Annals of the Institute of Statistical Mathematics*, 16(1), 1964.
- Kihyuk Sohn, Honglak Lee, and Xinchun Yan. Learning structured output representation using deep conditional generative models. *Advances in neural information processing systems*, 28, 2015.
- Kamilè Stankevičiūtė, Ahmed Alaa, and Mihaela van der Schaar. Conformal time-series forecasting. In *Advances in Neural Information Processing Systems*, 2021.
- Jennifer J Sun, Tomomi Karigo, Dipam Chakraborty, Sharada Mohanty, Benjamin Wild, Quan Sun, Chen Chen, David Anderson, Pietro Perona, Yisong Yue, et al. The multi-agent behavior dataset: Mouse dyadic social interactions. In *Thirty-fifth Conference on Neural Information Processing Systems Datasets and Benchmarks Track (Round 1)*, 2021.
- Yichuan Charlie Tang and Ruslan Salakhutdinov. Multiple futures prediction. *Advances in Neural Information Processing Systems*, 2019.
- Benjamin Ummenhofer, Lukas Prantl, Nils Thuerey, and Vladlen Koltun. Lagrangian fluid simulation with continuous convolutions. In *International Conference on Learning Representations*, 2019.
- Elise van der Pol, Daniel Worrall, Herke van Hoof, Frans Oliehoek, and Max Welling. Mdp homomorphic networks: Group symmetries in reinforcement learning. *Advances in Neural Information Processing Systems*, 33, 2020.
- Robin Walters, Jinxi Li, and Rose Yu. Trajectory prediction using equivariant continuous convolution. *International Conference on Learning Representations*, 2021.

- Rui Wang, Robin Walters, and Rose Yu. Incorporating symmetry into deep dynamics models for improved generalization. *International Conference on Learning Representations*, 2021.
- Shenlong Wang, Simon Suo, Wei-Chiu Ma, Andrei Pokrovsky, and Raquel Urtasun. Deep parametric continuous convolutional neural networks. In *Proceedings of the IEEE Conference on Computer Vision and Pattern Recognition (CVPR)*, June 2018.
- Maurice Weiler and Gabriele Cesa. General $E(2)$ -equivariant steerable CNNs. In *Advances in Neural Information Processing Systems (NeurIPS)*, 2019.
- Daniel E Worrall, Stephan J Garbin, Daniyar Turmukhambetov, and Gabriel J Brostow. Harmonic networks: Deep translation and rotation equivariance. In *Proceedings of the IEEE Conference on Computer Vision and Pattern Recognition*, 2017.
- Dongxia Wu, Liyao Gao, Xinyue Xiong, Matteo Chinazzi, Alessandro Vespignani, Yi-An Ma, and Rose Yu. Quantifying uncertainty in deep spatiotemporal forecasting. *ACM SIGKDD Conference on Knowledge Discovery and Data Mining (KDD)*, 2021.

Appendix A. Proofs

A.1. Proofs for Equivariance of Gaussians [Proposition 2]

In this section, we prove that the Gaussian probability density function is $\text{SO}(2)$ -equivariant.

Proposition *Given multivariate normal distribution $\mathcal{N}(\mu, \Sigma)$ over \mathbb{R}^2 with probability density function $p_{\mu, \Sigma}$ and $g \in \text{SO}(2)$, then $p_{g\mu, g\Sigma g^T}(v) = p_{\mu, \Sigma}(g^{-1}v)$ for all $v \in \mathbb{R}^2$.*

Proof

$$\begin{aligned} P_{g\mu, g\Sigma g^T}(v) &= \frac{1}{2\pi \det(g\Sigma g^T)} \exp\left(-\frac{1}{2}(v - g\mu)^T (g\Sigma g^T)^{-1}(v - g\mu)\right) \\ &= \frac{1}{2\pi \det(\Sigma)} \exp\left(-\frac{1}{2}(g^{-1}v - \mu)^T g^T g^{-T} \Sigma^{-1} g^{-1} g(g^{-1}v - \mu)\right) \\ &= \frac{1}{2\pi \det(\Sigma)} \exp\left(-\frac{1}{2}(g^{-1}v - \mu)^T \Sigma^{-1}(g^{-1}v - \mu)\right) \\ &= P_{\mu, \Sigma}(g^{-1}v) \end{aligned}$$

■

Proposition *Given a normal distribution $\mathcal{N}(\mu, \Sigma)$, its group-actioned $\mathcal{N}(g\mu, g\Sigma g^T)$ is also a valid normal distribution.*

Proof We prove the proposition by proving that $g\Sigma g^T$ is a symmetric positive definite matrix.

1) (Symmetry) $(g\Sigma g^T)^T = g^{TT} \Sigma^T g^T = g\Sigma g^T$.

2) (Positive Definite) Let $v \in \mathbb{R}^2$ and $v \neq 0$. Let $w = g^T v$, note that $w \neq 0$. Then $v^T g\Sigma g^T v = w^T \Sigma w > 0$, which implies Σ is a positive definite matrix. ■

A.2. Equivariance of construct for positive definite and symmetric Σ [Proposition 3]

Note that every positive definite symmetric matrix can be written as $\Sigma = MM^T$ for some $M \in \text{GL}_2(\mathbb{R})$, so we can represent Σ by a map φ where

$$\begin{aligned} \varphi: \text{GL}_2(\mathbb{R}) &\rightarrow \text{PosDefSym}_2(\mathbb{R}) \\ M &\mapsto MM^T \end{aligned}$$

Proposition φ is $\text{SO}(2)$ -equivariant.

Proof $\varphi(gMg^T) = gMg^T(gMg^T)^T = gMg^T g^{TT} M^T g^T = gMM^T g^T = g\varphi(M)g^T$ ■

We defined the one-sided inverse of φ as ψ :

$$\begin{aligned} \psi: \text{PosDefSym}_2(\mathbb{R}) &\rightarrow \text{GL}_2(\mathbb{R}) \\ \Sigma &\mapsto Q\lambda^{\frac{1}{2}} \end{aligned}$$

where $Q\lambda Q^T$ is the eigendecomposition of Σ and Q is orthogonal. That is, $\varphi(\psi(\Sigma)) = \Sigma$.

Proposition ψ is $\text{SO}(2)$ -equivariant.

Proof For symmetric positive definite matrix Σ , its eigenvector v_i and eigenvalue λ_i follows the eigenequation

$$\Sigma v_i = \lambda_i v_i.$$

For $\forall g \in \text{SO}(2)$,

$$g \Sigma v_i = \lambda_i g v_i \implies g \Sigma g^{-1} g v_i = \lambda_i g v_i \implies (g \Sigma g^{-1})(g v_i) = \lambda_i (g v_i),$$

so $g v_i$ is an eigenvector to $g \Sigma g^{-1}$, with corresponding eigenvalue λ_i .

Therefore,

$$\psi(g \Sigma) = g Q \Lambda^{\frac{1}{2}} = g \psi(\Sigma).$$

■

A.3. Proof of Proposition 1: The Equivariant Model Gives an Invariant Conditional Distribution.

We now prove Proposition 1.

Proposition [Proposition 1] If the one-step probabilistic forecasting model f_θ is G -equivariant, then the conditional probability distribution $p_\theta(\mathbf{x}_{t+1:t+k} | \mathbf{x}_{1:t}, \mathbf{e})$ is invariant as in Equation 2.

Proof Since $\mathbf{x}_{1:t}$ are known, we define $\Sigma_{1:t} = \epsilon \text{Id}$ for ϵ small approximating a delta distribution at $\mu_{1:t} = \mathbf{x}_{1:t}$. We then evaluate $\mu_{j+1}, \Sigma_{j+1} = f_\theta(\mu_{j-t+1:j}, \Sigma_{j-t+1:j}, \mathbf{e})$ autoregressively for $j = 1, \dots, k$. Finally define

$$\begin{aligned} p_\theta(\mathbf{x}_{t+1:t+k} | \mathbf{x}_{1:t}, \mathbf{e}) &= \prod_{j=1}^k p_\theta(\mathbf{x}_{t+j} | \mathbf{x}_{j:t+j-1}, \mathbf{e}) \\ &= \prod_{j=1}^k p_{N(\mu_{t+j}, \Sigma_{t+j})}(\mathbf{x}_{t+j}). \end{aligned} \tag{7}$$

For $g \in \text{SO}(2)$, we want to show

$$p_\theta(g \mathbf{x}_{t+1:t+k} | g \mathbf{x}_{1:t}, g \mathbf{e}) = p_\theta(\mathbf{x}_{t+1:t+k} | \mathbf{x}_{1:t}, \mathbf{e}).$$

Thus for $g \mathbf{x}_{1:t}, g \mathbf{e}$ we initialize $g \mu_{1:t}, g \Sigma_{1:t} g^T$ since $g \Sigma_{1:t} g^T = g g^T \Sigma_{1:t} = \Sigma_{1:t}$. Applying f_θ repeatedly and invoking equivariance, we obtain

$$g \mu_{t+j}, g \Sigma_{t+j} g^T = f_\theta(g \mu_{j:t+j-1}, g \Sigma_{j:t+j-1} g^T, g \mathbf{e}). \tag{8}$$

for $j = 1, \dots, k$. Then by Equation 7,

$$p_\theta(g \mathbf{x}_{t+1:t+k} | g \mathbf{x}_{1:t}, g \mathbf{e}) = \prod_{j=1}^k p_{N(g \mu_{t+j}, g \Sigma_{t+j} g^T)}(g \mathbf{x}_{t+j}).$$

Then by Proposition 2 this is

$$\prod_{j=1}^k p_{N(\mu_{t+j}, \Sigma_{t+j})}(g^{-1} g \mathbf{x}_{t+j}),$$

which cancels $g^{-1} g = 1$, and applying Equation 7 again gives $p_\theta(\mathbf{x}_{t+1:t+k} | \mathbf{x}_{1:t}, \mathbf{e})$. ■

A.4. Proof that MRS is a strictly proper scoring rule

Scoring rules are summary measures to evaluate probabilistic forecasts; they take in the forecasted distribution and the event or value that materializes and assign a numerical score. As defined in [Gneiting and Raftery \(2007\)](#), a scoring rule is proper if it is maximized when the forecaster recovers the ground truth distribution. It is strictly proper if the maximum is unique.

Proposition *MRS is a strictly proper score.*

Proof For arbitrary function h , we first define the scoring rule

$$S(R; z) = -|R| + \frac{1}{\alpha} (|R| - |R(z)|) \mathbb{1}\{z \in R^C\} + h(z),$$

which means if the forecaster quotes region R at the level $\alpha \in (0, 1)$ and z materializes, then the score $S(R; z)$ will be rewarded, where R and $R(z)$ are defined as ellipsoid parametric by μ and Σ . Then the expected score under the probability measure $P \in \mathcal{P}$ which z follows is defined as

$$S(R; P) = \int S(R; z) dP(z).$$

For $P \in \mathcal{P}$, let R_* denote the unique true P -region at level α . We say that scoring rule S is strictly proper if

$$S(R_*; P) \geq S(R; P),$$

for all region R and for all probability measures $P \in \mathcal{P}$, where equality holds if and only if $R = R_*$.

We identify P with the associated distribution function so that $P(R_*^C) = \alpha$. If $R_* \subset R$, then

$$\begin{aligned} S(R_*; P) - S(R; P) &= \int -|R_*| dP(z) + \frac{1}{\alpha} \int_{R_*^C} (|R_*| - |R(z)|) dP(z) \\ &\quad + \int |R| dP(z) - \frac{1}{\alpha} \int_{R^C} (|R| - |R(z)|) dP(z) \\ &= -|R_*| + |R| + \frac{1}{\alpha} |R_*| P(R_*^C) - \frac{1}{\alpha} |R| P(R^C) - \frac{1}{\alpha} \int_{R_*^C \setminus R^C} |R(z)| dP(z) \\ &\geq |R| - \frac{1}{\alpha} |R| P(R^C) - \frac{1}{\alpha} |R| (P(R_*^C) - P(R^C)) \\ &= 0, \end{aligned}$$

as it is supposed to be. If $R \subset R_*$, then an analogous argument applies.

Putting $h(z) = 0$ and reversing the sign of the scoring rule, yields the negatively oriented regional score. Finally, the mean score of this oriented regional score is our MRS, which is then proved to be proper. ■

Appendix B. Equivariant Matrix Output Layer Construction

Let

$$\rho_1(\theta) = \begin{pmatrix} \cos \theta & -\sin \theta \\ \sin \theta & \cos \theta \end{pmatrix} \quad M = \begin{pmatrix} a & b \\ c & d \end{pmatrix}$$

where a, b, c, d are trainable parameters. Consider input $f: S^1 \rightarrow \mathbb{R}$, then

$$F(f) = \int_{\theta=0}^{2\pi} f(\theta)\rho_1(\theta)M\rho_1(-\theta)d\theta.$$

Define $\rho_{reg}(\phi)(f)(\theta) = f(\theta - \phi)$.

Proposition *The convolution F is equivariant, i.e.,*

$$F(\rho_{reg}(\phi)f) = \rho_1(\phi)F(f)\rho_1(-\phi).$$

Proof We compute

$$\begin{aligned} F(\rho_{reg}(\phi)f) &= \int_{\theta=0}^{2\pi} \rho_{reg}(\phi)(f)(\theta)\rho_1(\theta)M\rho_1(-\theta)d\theta \\ &= \int_{\theta=0}^{2\pi} f(\theta - \phi)\rho_1(\theta)M\rho_1(-\theta)d\theta \\ &= \int_{u=-\phi}^{2\pi-\phi} f(u)\rho_1(u + \phi)M\rho_1(-u - \phi)du \quad (\text{substituting } u = \theta - \phi) \\ &= \rho_1(\phi) \cdot \left(\int_{u=-\phi}^{2\pi-\phi} f(u)\rho_1(u)M\rho_1(-u)du \right) \cdot \rho_1(-\phi) \\ &= \rho_1(\phi)F(f)\rho_1(-\phi). \end{aligned}$$

The last substitution follows from the fact the integrand is periodic of period 2π . Since the integral is over the whole circle, this equal to taking the limits of integration to be 0 and 2π . \blacksquare

Discretization. If the function f is discretized, such that $f_i = f(i2\pi/n)$. Then the mapping F is given by

$$F(f) = \sum_{i=0}^{n-1} f_i\rho_1(i2\pi/n)M\rho_1(-i2\pi/n).$$

Compatibility with matrix exponential For a $n \times n$ matrix M define

$$\exp(M) = \sum_{k=0}^{\infty} M^k/k!.$$

Matrix exponentiation is equivariant with respect to conjugation. That is for $g \in \text{GL}_n(\mathbb{R})$,

$$\exp(gMg^{-1}) = \sum_{k=0}^{\infty} (gMg^{-1})^k/k!.$$

Now note that

$$(gMg^{-1})^k = (gMg^{-1})(gMg^{-1}) \dots (gMg^{-1}) = gMM \dots Mg^{-1} = gM^k g^{-1}.$$

So then

$$\sum_{k=0}^{\infty} (gMg^{-1})^k/k! = \sum_{k=0}^{\infty} gM^k g^{-1}/k! = g \left(\sum_{k=0}^{\infty} M^k/k! \right) g^{-1} = g \exp(M)g^{-1}.$$

Structured Network Output So the last layers of the neural network will be $\exp \circ F$ which outputs an invertible 2×2 matrix and satisfies

$$(\exp \circ F)(\rho_{reg}(\phi)f) = \rho_1(\phi)(\exp \circ F)(f)\rho_1(-\phi).$$

Appendix C. Algorithms

C.1. Score Function for Probabilistic Forecast

We consider a probabilistic approach to trajectory forecasting. Ideally, we want the predicted distribution to be both sharp and valid under the definition in Equation 1. To quantify the uncertainty, we review the classic score function Mean Interval Score (MIS) and derive a 2 dimensional extension, Mean Regional Score (MRS).

Mean Interval Score. Mean Interval Score (MIS) is a proper scoring rule [Gneiting and Raftery \(2007\)](#) for interval forecasts that rewards narrower confidence intervals and encourages coverage. Specifically, let $Y \sim P_Y$ be a one-dimensional random variable, and an upper bound u , a lower bound l be its estimated $\frac{\alpha}{2}$ and $(1 - \frac{\alpha}{2})$ quantiles respectively, MIS is defined using samples $y_i \sim P_Y$.

$$\text{MIS}(u, l; Y) = \frac{1}{N} \sum_{i=1}^N [(u - l) + \frac{2}{\alpha}(y_i - u)\mathbb{1}\{y_i > u\} + \frac{2}{\alpha}(l - y_i)\mathbb{1}\{y_i < l\}]$$

Where the three terms in Equation 9 accounts for the width of the interval, and how much the sample point exceeds the upper bound and the lower bound, respectively. MIS has the advantage of being easy to compute and does not require the model to be parametric [Gneiting and Raftery \(2007\)](#). It can also be used as an objective function for probabilistic forecasting [Wu et al. \(2021\)](#).

Mean Regional Score. For n-D distributions, we introduce a new metric called the Mean Region Score (MRS), which generalizes MIS to higher dimensions. Let $Z \sim P_Z$ be an n-dimensional continuous random variable. First, we need to generalize α -quantile and define the confidence region. Let the region bordering z as $R(z)$, the confidence region of level α

$$R_P(\alpha) = \inf\{R(z) \mid \int_{R(z)} P(z)dz \geq \alpha\} \quad (9)$$

is the smallest region whose probability exceeds level α .

When the distribution is Gaussian $P_Z = \mathcal{N}(\mu, \Sigma)$ with mean $\mu \in \mathbb{R}^n$ and the covariance matrix $\Sigma \in \mathbb{R}^{2 \times 2}$ that is positive definite. The $(1 - \alpha)$ confidence region of an n-D multivariate normal distribution $P = \mathcal{N}(\mu, \Sigma)$ is an ellipsoid that can be written as ([Slotani, 1964](#)):

$$R(1 - \alpha) = \{z \mid (z - \mu)^T \Sigma^{-1} (z - \mu) \leq \chi_n^2(1 - \alpha)\}.$$

where χ_n^2 is the chi-squared distribution with n degrees of freedom. Then, for a given sample $z_i \in \mathbb{R}^n$, we can draw an ellipsoid whose edge coincides z_i defined as

$$R(z_i) = \{z \mid (z - \mu)^T \Sigma^{-1} (z - \mu) \leq c'\}$$

where $c' = (z_i - \mu)^T \Sigma^{-1} (z_i - \mu)$.

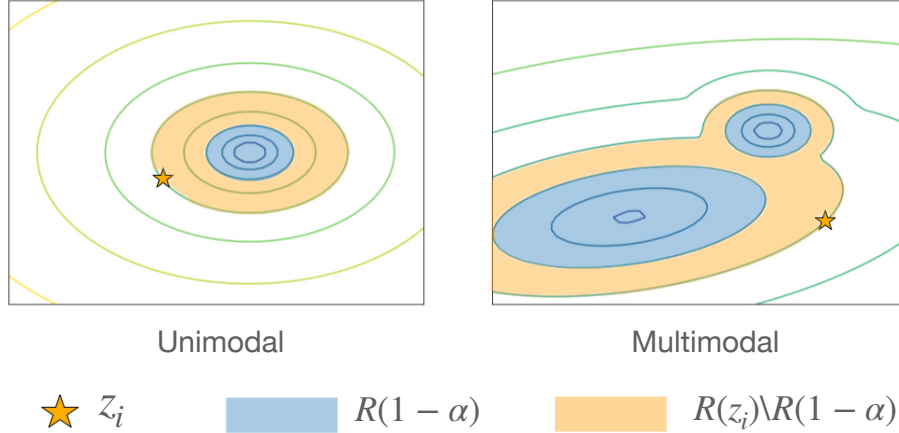


Figure 6: MRS illustration for unimodal and multimodal distributions. Given a sample z_i , MRS calculates the area of blue region plus that of the the orange region scaled by $1/\alpha$.

The MRS score of the $(1 - \alpha)$ prediction interval thus can be evaluated as:

$$\text{MRS}(R; Z) = \frac{1}{N} \sum_{i=1}^N [|R(1 - \alpha)| + \frac{1}{\alpha} |R(z_i) \setminus R(1 - \alpha)| \mathbb{1}\{z_i \in R^C(1 - \alpha)\}] \quad (10)$$

where the first term corresponds to the area of the confidence region and the second term measures how much each data z_i deviates from the region. $|\cdot|$ measures the size of the set. It is also easy to prove (see Appendix A.4) that MRS is a proper scoring rule [Gneiting and Raftery \(2007\)](#), which means MRS is optimized if and only if the distribution P recovers that of Z .

Figure 6 illustrates MRS for both unimodal and multimodal distributions. Note that when the distribution is single-modal, the confidence interval in Equation 10 is both *equally tailed* and the *shortest* confidence interval. For multi-modal distributions, we solve for the *smallest* confidence region to cover probable events. In appendix C.2 we present a method to estimate MRS for arbitrary 2-D distributions, where we divide the domain space into small grids to estimate density, and obtain $R(1 - \alpha)$ and $R(z_i)$ by assembling high density regions.

C.2. Empirical method for estimating MRS for general 2D distribution

We present an empirical method to estimate MRS given any 2D distribution. We first discretize the 2D space that is the domain of the probability distribution into n grid cells, indexing them as g_i where $i \in \{1, \dots, n\}$. Then we can numerically estimate the density of each grid cell $p(g_i)$ for $i = 1, \dots, n$. The confidence region can be estimated by selecting the grid cells with the highest likelihoods until they sum to $1 - \alpha$.

$$R(1 - \alpha) = \bigcup_{i \in K} g_i, \quad K = \text{argmin}_K : \sum_{i \in K} p(g_i) \geq 1 - \alpha$$

where K is the superlevel set of grid cells g_i whose empirical probability density is at least $1 - \alpha$.

Similarly, we define the estimated region

$$R(z_i) = \bigcup_{p(g_i) \geq p(z_i)} g_i$$

as the superlevel set of data point z_i . This way, we can calculate MRS for any 2D using the estimated $R(1 - \alpha)$ and $R(z_i)$ in the MRS formula.

$$\text{MRS}(R; Z) = \frac{1}{N} \sum_{i=1}^N [|R(1 - \alpha)| + \frac{1}{\alpha} |R(z_i) \setminus R(1 - \alpha)| \mathbb{1}\{z_i \in R^C(1 - \alpha)\}]$$

Figure 7 illustrates the idea, this method is used to estimate the MRS scores for multimodal methods `Trajectron++` and `MFP` in our experiments.

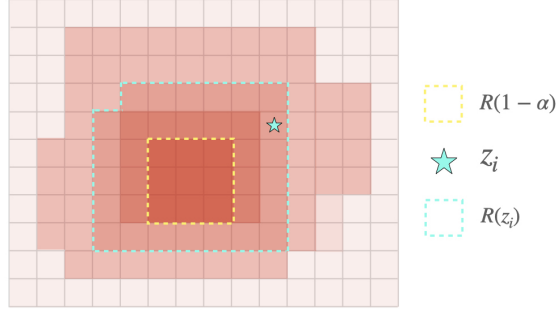


Figure 7: Illustration for empirical MRS estimation, where we calculate the probability density at each grid, and select the highest density grids to construct $R(z_i)$ and $R(1 - \alpha)$. This way, we may approximate MRS numerically.

C.3. Conformal algorithm for 2-D Time Series

We extend the inductive conformal prediction (ICP) algorithm [Shafer and Vovk \(2008\)](#) to conformally estimate a confidence region for 2D forecasts. Given an exchangeable set of trajectory observations $\mathcal{D} = \{(\mathbf{x}_{1:t}^{(i)}, \mathbf{e}^{(i)}), \mathbf{x}_{t+1:t+k}^{(i)}\}_{i=1}^l$ and a new sample $(\mathbf{x}_{1:t}^{(l+1)}, \mathbf{e}^{(l+1)})$, the ICP algorithm returns k prediction intervals, $[\Gamma_1^\alpha, \dots, \Gamma_k^\alpha]$, one for each timestep, such that:

$$\mathbb{P}[\forall j \in \{1, \dots, k\}, x_{t+j} \in \Gamma_j^\alpha(\mathbf{x}^{(l+1)})] \geq 1 - \alpha$$

for any underlying predictive model. This inequality is the *validity* condition. [Stankevičiūtė et al. \(2021\)](#) proves the 1-D case for time-series forecasting validity; we leave proving it for the 2-D case for future work.

ICP requires an underlying forecasting model and a choice of nonconformity score. In our case, LSTM and ECCO are both models that take as input $(\mathbf{x}_{1:t}, \mathbf{e})$ and outputs $\mathbf{x}_{t+1:t+k}$. We select root mean square error (RMSE) as our nonconformity score as it is commonly used in the 1-d setting and naturally extends to high dimensions. We split the training set into the proper training set and a calibration set of equal size: $\mathcal{D} = \mathcal{D}_{train} \cup \mathcal{D}_{cal}$. We train our model M on \mathcal{D}_{train} and obtain the critical nonconformity scores $\hat{\gamma}_1, \dots, \hat{\gamma}_k$ as in algorithm 1 in [Stankevičiūtė et al. \(2021\)](#). Then, for input $(\mathbf{x}_{1:t}, \mathbf{e})$ and $\hat{x}_{t+1:t+k} = M(\mathbf{x}_{1:t}, \mathbf{e})$ we can construct a set of confidence intervals

$$\Gamma_j^\alpha(\mathbf{x}_{1:t}^{(l+1)}) = \{x \in \mathbb{R}^2 \mid \text{RMSE}(x, \hat{x}_j) \leq \hat{\gamma}_j\} \text{ for } j \in \{1, \dots, k\}$$

We illustrate some example scenes with confidence regions provided by conformal-ECCO in figure 8. Note that the regions for timestep j are given by $\hat{\gamma}_j$, hence are the same for every scenario.

With our choice of RMSE as the nonconformity score, the region is a circle; they appear elliptical due to scale compression.

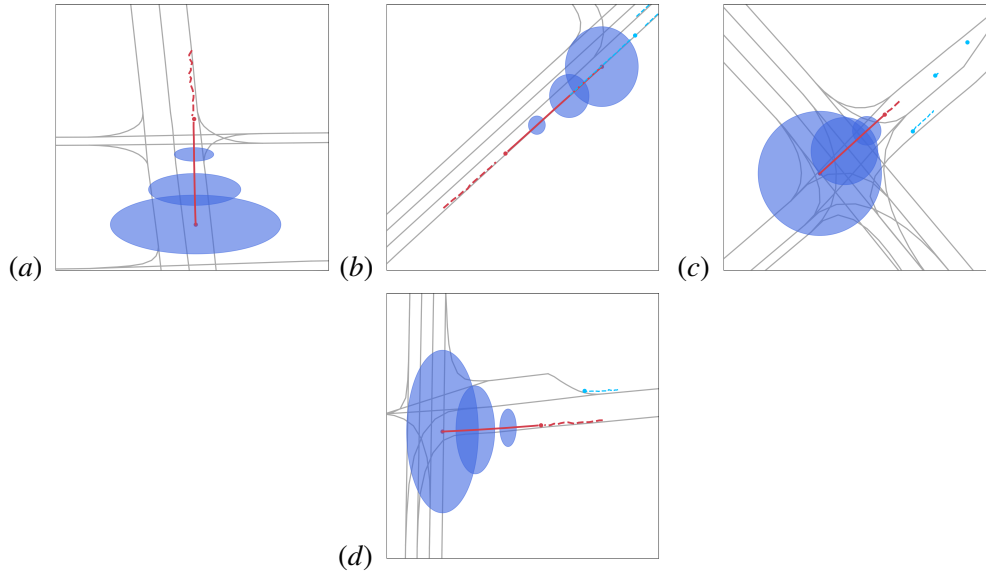


Figure 8: Scene illustrations for confidence regions given by conformal-ECCO. Note that in order to achieve 90% coverage, the region is larger than needed, especially in straight-lane cases like left two scenarios. Due to the lack of underlying assumption about the distribution, the model isn't able to adjust the shape of uncertainty according to data either.

Appendix D. Experiment Details

D.1. Implementation Details

The numbers in [Table 2](#) are reported on the official validation set for Argoverse, and on a 10% test split for TrajNet++. For the particle dataset, the reported numbers are also on a 10% test split.

Dataset and Preprocessing The synthetic particle dataset is generated by the spring dynamics simulator in [Kipf et al. \(2018\)](#). We added $\sigma = 0.01$ noise to the dynamics each step to introduce some uncertainty. The dataset consists of 12,000 time series of trajectories of 5 interacting particles over 50 timesteps ; we use 30 steps as input and predict the following 20 steps. 1,000 samples are used for model validation and 1,000 are used for testing.

The Argoverse autonomous vehicle dataset contains 205,942 samples, consisting of diverse driving scenarios from Miami and Pittsburgh. We split 90/10 into a training set and validation set of size 185,348 and 20,594 respectively. The official validation set of size 39,472 is used for testing and reporting performance. We preprocess the scenes to filter out incomplete trajectories and cap the number of vehicles modeled to 60. If there are less than 60 cars in the scenario, we insert dummy cars into them to achieve consistent car numbers. For map information, we only include center lanes with lane directions as features. Similar to vehicles, we introduce dummy lane nodes into each scene to make lane numbers consistently equal to 650.

We use the latest release of the TrajNet++ dataset (Update 4.0) for our pedestrian experiments. TrajNet++ is a compiled set of pedestrian trajectories captured in both indoor and outdoor locations such as in universities, hotels, Zara, and train stations. The sample in this dataset is 21 timestamps long, and the goal is to predict the 2D spatial positions for each pedestrian in the future 12 timestamps given the first 9. The pedestrian dataset contains 240,896 samples, which we split 80/10/10 into train, validation, and test sets. Similar to Argoverse, we filter out incomplete trajectories in processing and either cap or insert dummy pedestrians such that each scene has 60 agents. No map information was used in the pedestrian dataset.

We include our code for preprocessing, model implementation, and training in the supplementary materials.

Hyperparameters and Training Details We trained the PECCO model with 4 equivariant continuous convolution layers of hidden size of (8, 16, 16, 16) respectively for Argoverse, and (4, 8, 16, 16) for the Trajnet++ pedestrian dataset. Our models are all trained with Adam optimizer with a base learning rate $r = 0.001$, and linear learning rate scheduler set to $\gamma = 0.95$. For Argoverse task, we set the CtsConv radius to be 40, and for the pedestrian task we set it to be 6. PECCO’s Argoverse model has 129k parameters. For comparison, Trajectron++ has 127k and MFP has 67K.

All our models without map information are trained for 10K iterations with batch size 32 with learning rate updating every 150 iterations. Most of our experiments are performed on a server with 4 RTX 2080 Ti GPUs, and it takes around 9-12 hours to finish training. We run each experiment 3 times with different random initialization and data order. The numbers reported in tables 2, 3, and 6 are the mean and standard deviation of those 3 runs.

D.2. Deterministic Baseline Results

We present numbers for deterministic baseline models for Argoverse and Trajnet++. By sampling, we achieve better minADE/minFDE performance with probabilistic models, but they serve as valuable baselines to illustrate the difficulty of the task.

Model	Argoverse		Trajnet++	
	ADE↓	FDE↓	ADE↓	FDE↓
Constant Velocity	2.77	6.16	1.21	2.37
Nearest Neighbor	3.52	7.85	1.25	2.61
LSTM	1.97 ± .05	4.98 ± .31	1.01 ± .02	1.98 ± .08
CtsConv	1.87 ± .06	4.43 ± .28	1.35 ± .05	2.97 ± .16
ECCO	1.68 ± .04	3.98 ± .19	0.94 ± .01	2.05 ± .03

Table 6: Deterministic baselines on the Argoverse and TrajNet++ dataset